AERODYNAMICS OF SINGLE AND MULTIPLE ROTORS HOVERING INSIDE A SQUARE TUNNEL

Yasutada Tanabe, tan@chofu.jaxa.jp, JAXA (Japan)
Hideaki Sugawara, hideaki8@chofu.jaxa.jp, Ryoyu Systems (Japan)
Shigeru Sunada, shigeru.sunada@mae.nagoya-u.ac.jp, Nagoya University (Japan)
Koichi Yonezawa, koichi-y@criepi.denken.or.jp, CRIEPI (Japan)
Hiroshi Tokutake, tokutake@se.kanazawa-u.ac.jp, Kanazawa University (Japan)

Abstract

Flight performances of hovering single and multiple rotors inside tunnels are studied. Following the wide spread of applications of the multiple rotor type drones, possible observation and search inside tunnels are under investigations. With constraints of the surrounding walls in a narrow tunnel, there is concern that the downwash caused by the hovering rotors may circulate around the aircraft and the flight performance may be severely deteriorated. In this numerical simulation study, a single rotor and a hexa-rotor UAV are placed inside straight square tunnels with various width. It is found that when the gap between the rotor tip and the wall is less than two diameters of the rotor, the hover performance is severely degraded.

1. INTRODUCTION

The multiple rotor type drones (multicopters) with a gross weight less than 10 kg are widely applied to photographing, observation, reconnaissance, and other missions. Larger multicopters with a gross weight ranging from 10 to 100 kg are developed for agricultural spraying and other industrial utilities. Recently, multicopters with even heavier gross weight are under development for passenger carrying. [1] Most of the multicopters adopt simple fixed pitch-angle propellers and flight is controlled through the rotational speed change of the rotors which are directly connected to electrically driven motors. There is no swashplate or other complicated mechanical components onboard.

To improve the gust tolerance of the multicopters, as a part of the Tough Robotics Challenge (TRC) of the ImPACT Program [2] the authors have tested a series of prototypes of variable pitch-angle propellers. With the sacrifice of the mechanical simplicity by adding a pitch-angle change actuator to each propeller, much faster thrust change of the propeller can be achieved. These prototypes have been successfully applied to bridge maintenance checks. It is expected that for the observation missions near a structure where strong wind shears and gusts exist, this type of fast response multicopters will be suitable and applicable.

The interactions between the rotors may cause vibrations and the overall aerodynamic performance is also influenced by the distances between the rotors. [3] When a multicopter is flying near a wall, strong interaction between the flowfield around the rotors and the wall can occur. It is suggested that at least a distance of 2 times of the rotor diameter should be kept away from a side wall or an upper wall to avoid the influence of the wall. [4, 5]

There are also needs to fly multicopters to observe through tunnels where pipes and/or electric cables are running, or along water channels of hydraulic power plants. With the constraints of the surrounding walls in a narrow tunnel, there is concern that the downwash caused by the hovering rotors may circulate around the aircraft and the flight performance may be severely deteriorated. Numerical simulations of a single rotor and hexa-rotors hovering inside tunnels of various sizes with a square section are carried out. The rotor hovering performance with the size of the tunnels are investigated.

2. ROTOR MODEL

The rotor model simulated is based on the 1st prototype of the variable pitch-angle controlled multicopter as shown in Figure 1. The design parameters are listed in Table 1 and the notation definitions is shown in Figure 2. The rotor diameter is 0.33 m and the blade number is 2 with a tapered planform. The airfoil is NACA0009 and there is no twist. The nominal rotor tip speed is 100 m/s and the Reynolds number based on the chord length is about 2.0×10^5.

The aerodynamic forces and moments acting on the multicopter are calculated based on Equation (1) where the aircraft center is placed at the center of the six rotors. Nondimensionalizations are defined as shown in Equation (2).

Presented at 44th European Rotorcraft Forum, Delft, The Netherlands, 19-20 September, 2018

Figure 1: A variable pitch-angle controlled multicopter prototype

Table 1: Design parameters of the rotor blade

Design Parameters	
Number of rotors, N_R	6
Rotor center distance, L	0.393 m
Rotor diameter, D	0.330 m
Rotor radius, R	0.165 m
Chord length, c_{root}, c_{tip}	c_{root} = 0.048 m c_{tip} = 0.029 m
Blade planform	Tapered
Blade twist	0 deg
Blade airfoil	NACA0009
Number of blade, N_b	2
Tip Mach number, M_{tip}	0.29412 (100 m/s)
Reynolds number based on chord length	1.99x10^5

$$
\begin{aligned}
X_{sum} &= \sum_{i=1}^{6} X_i \\
Y_{sum} &= \sum_{i=1}^{6} Y_i \\
Z_{sum} &= \sum_{i=1}^{6} Z_i \\
Mx_{sum} &= \sum_{i=1}^{6} Mx_i + \sum_{i=1}^{6} Z_i y_i \\
My_{sum} &= \sum_{i=1}^{6} My_i + \sum_{i=1}^{6} -Z_i x_i \\
Mz_{sum} &= \sum_{i=1}^{6} Mz_i + \sum_{i=1}^{6} \{-X_i y_i + Y_i x_i\}
\end{aligned}
\qquad (1)
$$

$$
\begin{aligned}
C_X &= F_X / \left(\rho \pi R^2 V_{tip}^2\right) \\
C_Y &= F_Y / \left(\rho \pi R^2 V_{tip}^2\right) \\
C_Z &= C_T = F_Z / \left(\rho \pi R^2 V_{tip}^2\right) \\
C_{MX} &= M_X / \left(\rho \pi R^2 V_{tip}^2 R\right) \\
C_{MY} &= M_Y / \left(\rho \pi R^2 V_{tip}^2 R\right) \\
C_{MZ} &= -C_Q = M_Z / \left(\rho \pi R^2 V_{tip}^2 R\right) \\
C_P &= P / \left(\rho \pi R^2 V_{tip}^3\right) = C_Q
\end{aligned}
\qquad (2)
$$

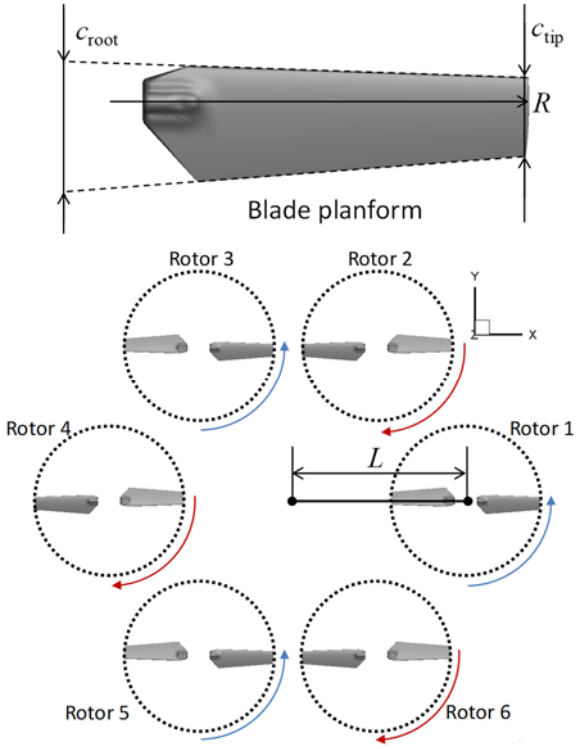

Figure 2: Definition of design parameters of the rotor

3. NUMERICAL METHODOLOGIES

Numerical simulations of the rotors hovering inside tunnels are performed using a CFD code, rFlow3D, developed in JAXA for rotorcraft. In the rFlow3D code,[6, 7] a three dimensional moving overlapping grid method is used. This code is originally developed to treat the conventional helicopters where a main rotor and a tail rotor are considered. For the multicopters, quad, hexa, octo and even more rotors are used. The data structure in rFlow3D is changed so that a multicopter with any number of rotors can be handled. Any number of inner background grids can also be placed for efficient capturing of the rotor near-wakes.

The full Navier-Stokes equation in ALE form is solved. An all-speed numerical scheme SLAU

Presented at 44th European Rotorcraft Forum, Delft, The Netherlands, 19-20 September, 2018

(Simple Low-dissipation AUSM) [8] with extension to three dimensional moving grids (referred as mSLAU) is adopted. [9] It is very suitable for the flow calculation around a rotary wing, where the local flow speed may vary from very low on the root area to transonic at the tip. Combining SLAU with a Fourth-order Compact MUSCL TVD (FCMT) interpolation scheme, [10] fourth-order spatial accuracy is obtained in shock free regions. Implicit LU-SGS and Dual-Time-Stepping method [11] are used for time integration on blade grids. Yet for the background grids, explicit four stages Runge-Kutta time integration method [12] is used. In this study, considering the relative low Reynolds numbers on the rotors, no turbulence model is applied. The adopted numerical methods are listed in Table 2.

Table 2: CFD methodologies

Items	Background Grids	Blade Grids
Governing equations	3D compressible Navier-Stokes equations	
Spatial discretization	Cell-vertex FVM	Cell-centered FVM
Time integration	4 stages Runge-Kutta method	Dual-time stepping / LU-SGS Implicit method
Inviscid flux	mSLAU numerical scheme	
Reconstruction	FCMT (Fourth Order Compact MUSCL TVD) method	
Viscous terms	2nd order central differences	
Turbulence model	-	-

4. NUMERICAL SETTINGS

The tunnel models are with square section. The four surrounding walls are flat and the tunnels are unlimitedly long as shown in Figure 3. The single rotor or the multicopter is hovering at the section center.

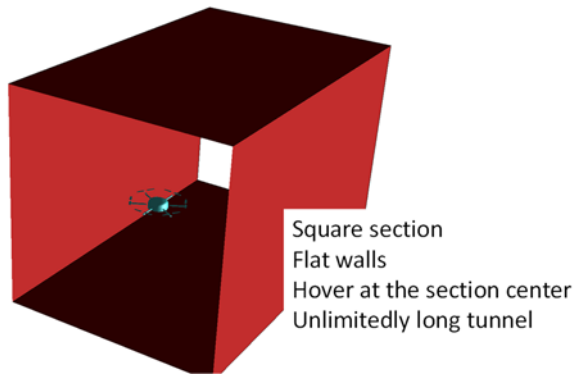

Figure 3: Tunnel model with square section

Based on the notations defined in Figure 4, the hexa-rotors are fixed at a pitch angle of 10 degrees. 6 test cases are simulated with the distances between the rotor tip and the wall varies from 1 R to 10 R as listed in Table 3.

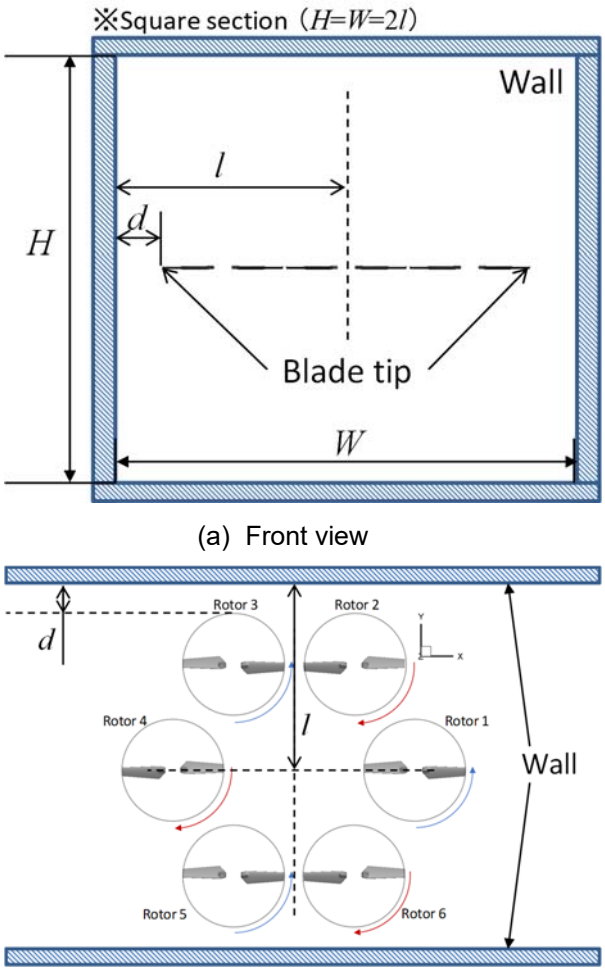

Figure 4: Notations used for hexa-rotors inside tunnels

Table 3: Test cases for hexa-rotors inside tunnels

Case No.	Pitch angle θ_0	Distance between rotor tip and wall, d	d/R	d/D	l/D
1	10°	0.165	1.0	0.5	2.03
2		0.33	2.0	1.0	2.53
3		0.66	4.0	2.0	3.53
4		0.99	6.0	3.0	4.53
5		1.32	8.0	4.0	5.53
6		1.65	10.0	5.0	6.53
7		Without Wall	-	-	-

The blade grid and the inner background grid are common for all the cases. An equal spacing of 20% of the blade tip chord length is used on the inner background grid. The outer background grid as shown in Figure 5 is constructed depending on the wind tunnel width. Minimum grid height on the tunnels walls is 0.001 m to resolve the boundary layers formed on the walls.

Presented at 44th European Rotorcraft Forum, Delft, The Netherlands, 19-20 September, 2018

The grid points for each test case are shown in Table 4.

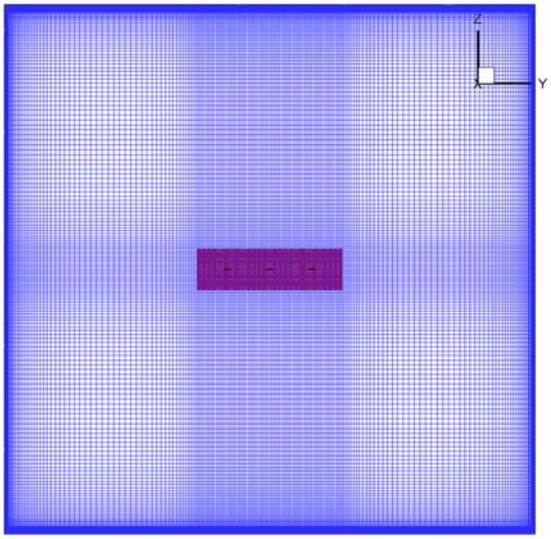

Figure 5: Outer background grid inside the tunnel section

Table 4: Grid points for each test cases

	Single Rotor	Hexa-Rotors
Blade grid	91 x 101 x 51 (468,741)	
Inner Background (IBK) grid	85 x 85 x 57 (411,825)	221 x 205 x 57(2,582,385)
OBK grid (w/o wall)	157 x 175 x 183 (5,027,925)	211 x 269 x 223 (12,657,257)
OBK grid (d=1.0R)	157 x 67 x 91 (957,229)	221 x 123 x 183 (4,974,489)
OBK grid (d=2.0R)	157 x 83 x 103 (1,342,193)	211 x 183 x 203 (7,838,439)
OBK grid (d=4.0R)	157 x 115 x 123 (2,220,765)	211 x 183 x 203 (7,838,439)
OBK grid (d=6.0R)	157 x 135 x 143 (3,030,885)	211 x 203 x 203 (8,695,099)
OBK grid (d=8.0R)	157 x 155 x 163 (3,966,605)	211 x 203 x 223 (9,551,759)
OBK grid (d=10.0R)	157 x 175 x 183 (5,027,925)	211 x 223 x 223 (10,990,109)

5. RESULTS AND DISCUSSSIONS

5.1. A Single Rotor Inside Tunnels

Velocity vectors on the cross section caused by a single rotor for various distances between the rotor tip and the side walls are shown in Figure 6. The w/o-wall case is shown for comparison. When the d/D is 0.5, the flowfield around the rotor is remarkably unsteady and the circulated flow is oscillating.

Thrust of the rotor is clearly affected by the tunnel width as shown in Figure 7. Even with the widest size (11 times of the rotor diameter) of the tunnel, the thrust is about 1% lower than the w/o-wall case. Smaller tunnel corresponding to lower thrust when the rotor blade pitch angle is fixed at 10 degrees. The Figure of Merit of the single rotor inside the tunnels is a little improved about 1% when the gap is greater than 2 diameters. When the rotor tip gap with the wall is less than 1 diameter, the thrust decreases abruptly. Similar changes are observed for the torque and the Figure of Merit (FM) in Figure 8 and Figure 9 respectively. Even lower torque is required for lower thrust, the rotor Figure of Merit is degraded more than 10% when the tip gap is changed from 5 D to 0.5 D.

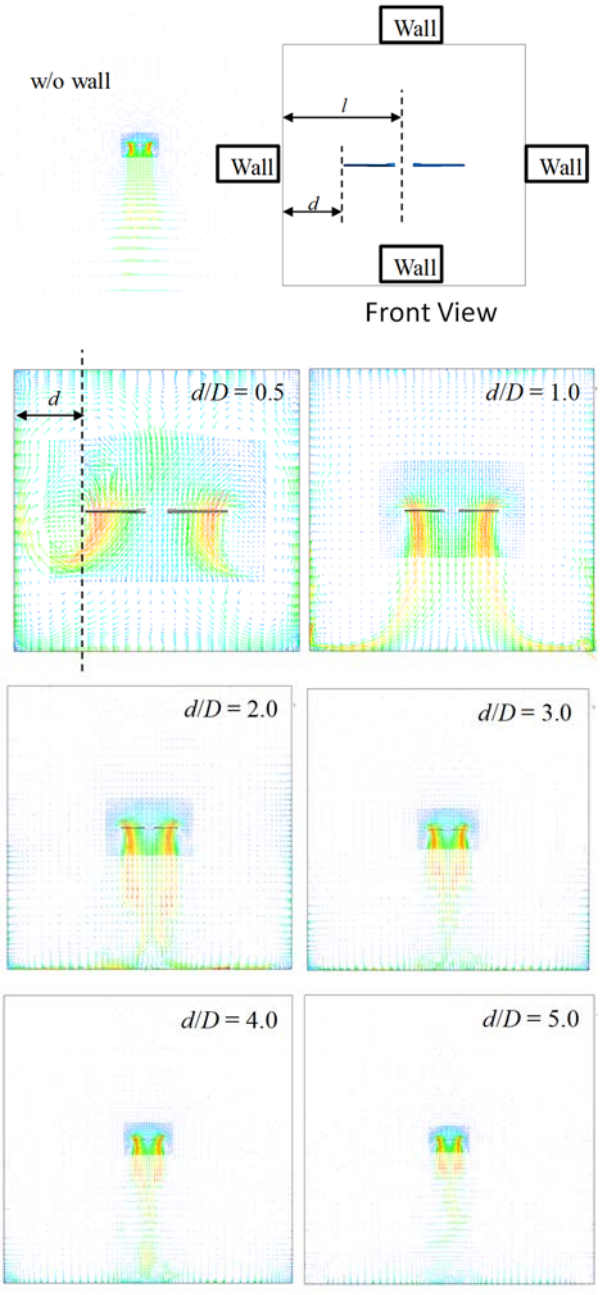

Figure 6: Velocity vectors caused by a hovering single rotor inside tunnels

Presented at 44th European Rotorcraft Forum, Delft, The Netherlands, 19-20 September, 2018

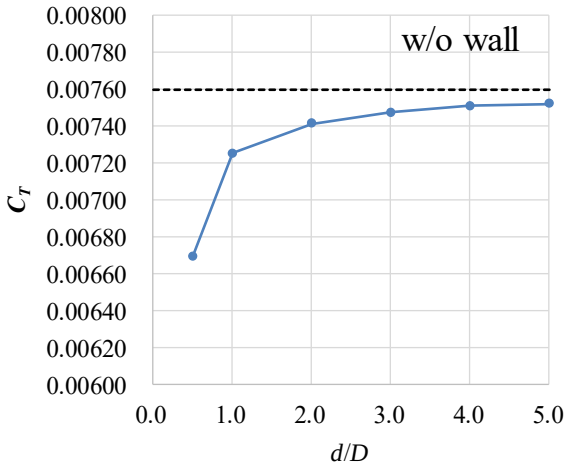

Figure 7: Thrust change with distance between rotor-tip and the side wall for a single rotor

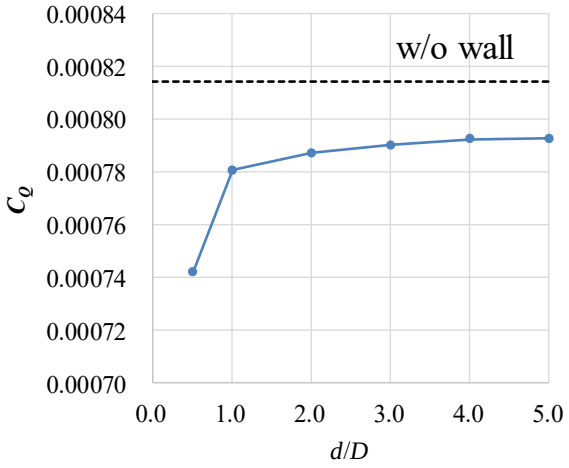

Figure 8: Torque coefficient change with distance between rotor-tip and the side wall for a single rotor

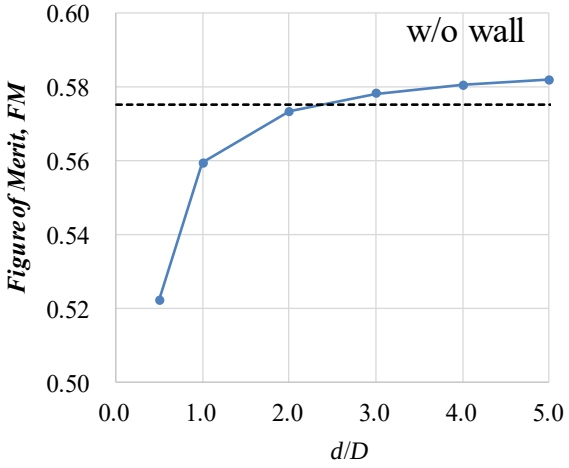

Figure 9: Rotor Figure of Merit (FM) change with distance between rotor-tip and the wall for a single rotor

5.2. Hexa-Rotors inside tunnels

For the hexa-rotors, the velocity vectors are shown on Section 1 and Section 2 as illustrated in Figure 10. Section 2 is along the tunnel centreline.

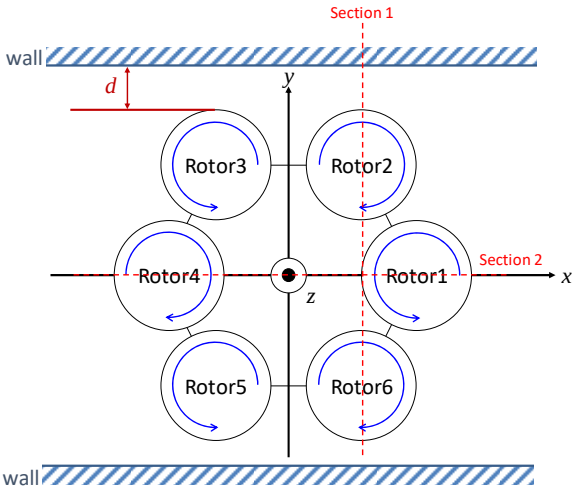

Figure 10: Illustration of Section 1 and Section 2 for hexa-rotors inside tunnels

The velocity vectors on section 1 are shown in Figure 11. It is observed that when the tip gap *d* is less than 2 rotor diameters, the flows on the cross section are significantly unsteady. The w/o wall case is also shown here for comparison.

The velocity vectors on section 2 are shown in Figure 12. Flow along the bottom surface to both sides can be observed.

The averaged thrust change with the rotor tip gap with the wall is shown in Figure 13. Different from the single rotor case, the thrust is nearly the same or even a little higher than the w/o wall case when the gap is larger than 2 rotor diameters. When the gap is less than 2 rotor diameters, the thrust decreases abruptly.

The averaged required torque is shown in Figure 14, which is lower than the w/o wall case about 3% when the gap is larger than 2 times of the rotor diameter. The improvement of the rotor performance inside a relative large tunnel is considered due to the ground effect.

The averaged rotor Figure of Merit (FM) is shown in Figure 15. When the gap is larger than 2 rotor diameters, the FM is better than the w/o wall case about 3%. However, when the gap is less than 2 rotor diameters, FM decreases abruptly. It is suggested that the multicopter will be difficult to hover inside a tunnel when the rotor tip gap is less than 2 rotor diameters.

Presented at 44th European Rotorcraft Forum, Delft, The Netherlands, 19-20 September, 2018

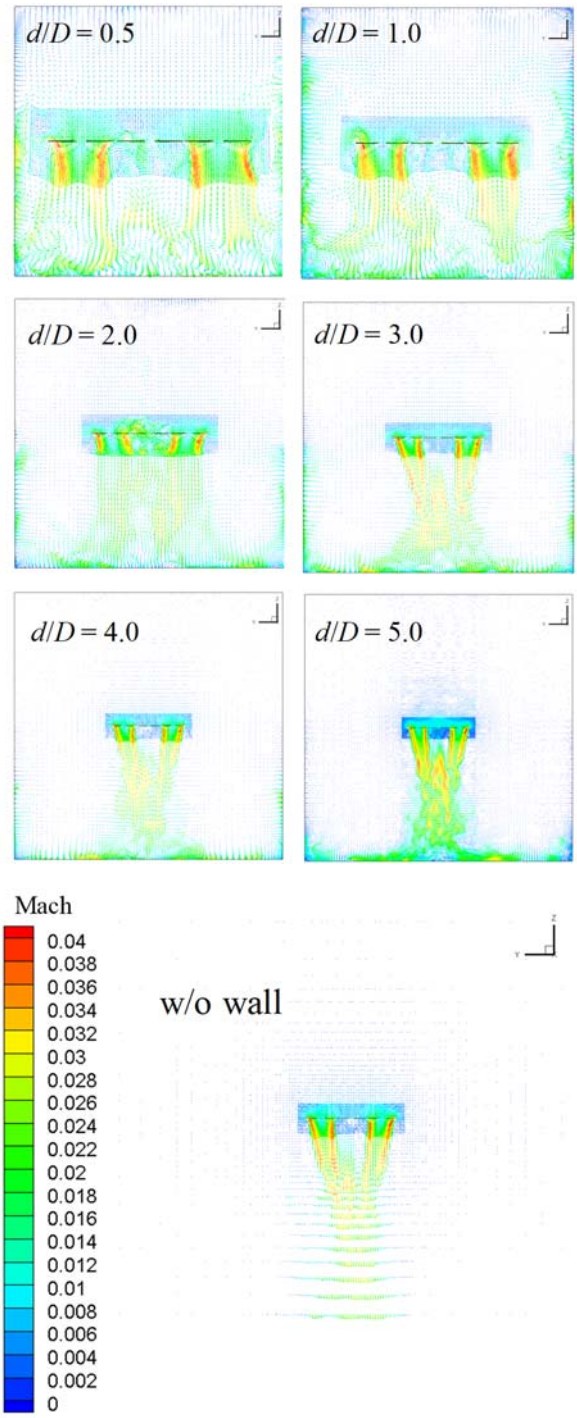

Figure 11: Velocity vectors on Section 1 for different distances between rotor-tip and the wall.

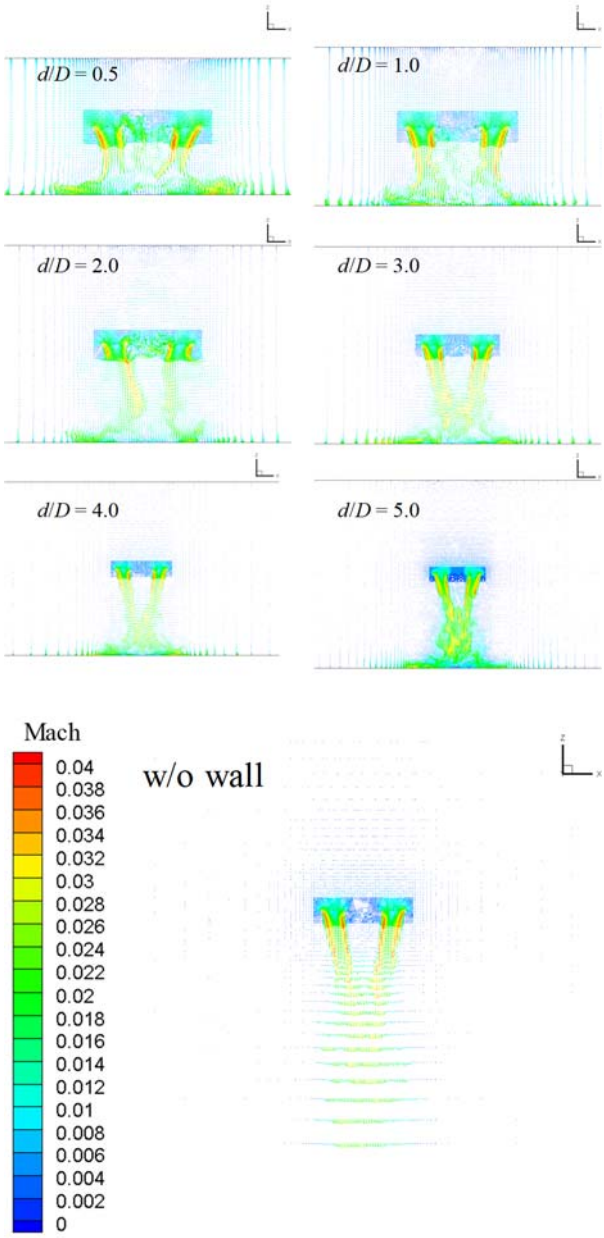

Figure 12: Velocity vectors on Section 2 for different distances between rotor-tip and the wall.

Presented at 44th European Rotorcraft Forum, Delft, The Netherlands, 19-20 September, 2018

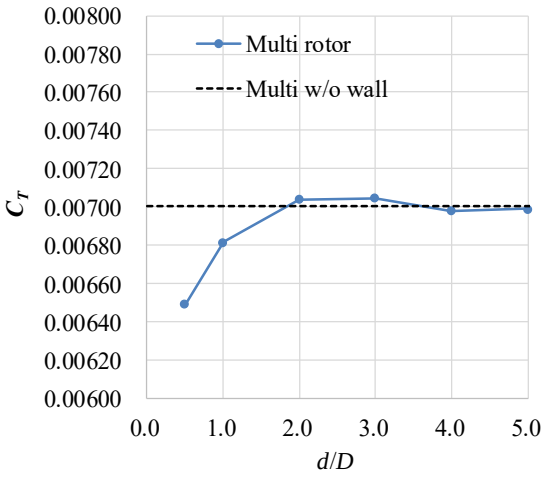

Figure 13: Averaged rotor thrust coefficient change with the distance between the rotor-tip and the wall

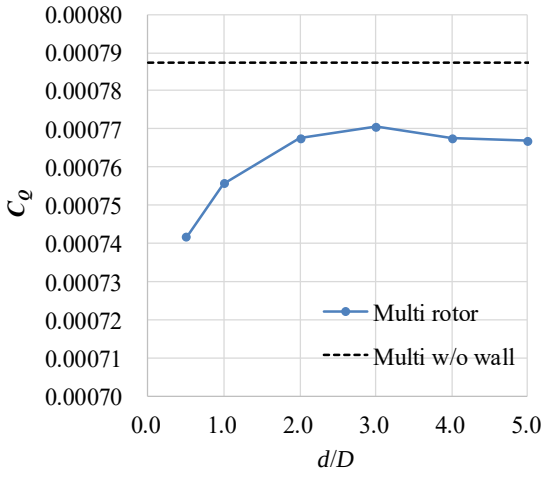

Figure 14: Averaged rotor torque coefficient change with the distance between the rotor-tip and the wall

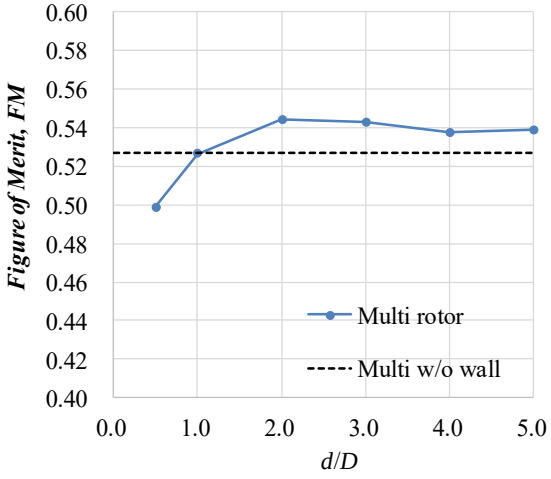

Figure 15: Averaged rotor Figure of Merit (FM) change with the distance between the rotor-tip and the wall

6. SUMMARIES

Based on a prototype variable pitch-angle controlled multicopter, a single rotor and hexa-rotors hovering at the section center inside square tunnels are numerically simulated. The rotor performance change with the size of the tunnels is investigated.

For a single rotor inside a tunnel, the rotor performance is continuously degraded when the tunnel size is narrowing. The hovering performance is severely worsening when the distance between the rotor tip and the wall is less than 1 diameter (the tunnel section is less than 3 diameters square).

For the hexa-rotors, the flowfields around the rotors are complicated and unsteady. When the distance between the rotor tip and the wall is less than 2 diameters of the rotor, the thrust generated by the rotors at a fixed pitch angle start to decrease and the rotor performance is degraded.

The section shape and the position where the multicopter is hovering are considered to have significant influences on the aerodynamic performance of the rotors. Numerical simulations based on real situations will be carried out.

ACKNOWLEDGMENT

This research was funded by ImPACT Program of Council for Science, Technology and Innovation (Cabinet Office, Government of Japan)

REFERENCES

[1] Electric VTOL News™ by the Vertical Flight Society, http://evtol.news, accessed on August 5, 2018.

[2] The Japan Science and Technology Agency (JST), ImPACT: Impulsing Paradigm Change through Disruptive Technologies Program, Tough Robotics Challenge (TRC), http://www.jst.go.jp/impact/en/ program/ 07. html, accessed on Feb. 21, 2018.

[3] Y. Tanabe, T. Aoyama, M. Sugiura, H. Sugawara, S. Sunada, K. Yonezawa, and H. Tokutake, Numerical Simulations of Aerodynamic Interactions Between Multiple Rotors, 42nd ERF, Lille, France, Sept. 6-9, 2016.

[4] Y. Tanabe, M. Sugiura, T. Aoyama, H. Sugawara, S. Sunada, K. Yonezawa, and H. Tokutake, Influences of Upper and Side Walls on the Performance of a Multiple Rotor Drone, 6th Asian-Australian Rotorcraft Forum & Heli Japan 2017, Kanazawa, Ishikawa, Japan, Nov. 7-9, 2017.

Presented at 44th European Rotorcraft Forum, Delft, The Netherlands, 19-20 September, 2018

[5] Y. Tanabe, M. Sugiura, T. Aoyama, H. Sugawara, S. Sunada, K. Yonezawa, and H. Tokutake, Multiple Rotors Hovering Near an Upper or a Side Wall, Journal of Robotics and Mechatronics, Vol. 30, No. 3, pp. 344-353, 2018.

[6] Y. Tanabe, S. Saito and H. Sugawara, Construction and Validation of an Analysis Tool Chain for Rotorcraft Active Noise Reduction, 38th ERF, Amsterdam, NL, Sept. 4-7, 2012.

[7] Y. Tanabe, S. Saito, O. Takayama, D. Sasaki, and K. Nakahashi, A New Hybrid Method of Overlapping Structured Grids Combined with Unstructured Fuselage Grids for Rotorcraft Analysis, 36th European Rotorcraft Forum, Paris, France, September 9-11, 2010.

[8] Y. Tanabe, and S. Saito, Significance of All-Speed Scheme in Application to Rotorcraft CFD Simulations, The 3rd International Basic Research Conference on Rotorcraft Technology, Nanjing, China. October, 2009.

[9] S. Yamamoto, and H. Daiguji, Higher- Order-Accurate Upwind Schemes for Solving the Compressible Euler and Navier-Stokes Equations, Computers & Fluids, Vol.22, No.2/3, pp.259-270, 1993.

[10] E. Shima, and K. Kitamura, On New Simple Low-Dissipation Scheme of AUSM-Family for All Speeds, 47th AIAA Aerospace Sciences Meeting, Orlando, FA, January 5-8 2009, AIAA Paper 2009-136.

[11] L.P. Zhang, and Z.J. Wang, A Block LU-SGS Implicit Dual Time-Stepping Algorithm for Hybrid Dynamic Meshes, Computers & Fluids, Vol.33, pp.891–916, 2004.

[12] A. Arnone, M.S. Liou, and L. A. Povinelli, Multigrid Time-Accurate Integration of Navier-Stokes Equations, NASA TM-106373, November 1993.

Presented at 44th European Rotorcraft Forum, Delft, The Netherlands, 19-20 September, 2018